JOURNAL OF GEOPHYSICAL RESEARCH, VOL. 112, D20114, doi:10.1029/2007JD008612, 2007

Potassium lidar temperatures and densities in the mesopause region at Spitsbergen (78°N)

J. Höffner[1] and F.-J. Lübken[1]

Received 5 March 2007; revised 14 June 2007; accepted 20 July 2007; published 25 October 2007.

[1] Lidar measurements of potassium temperatures and number densities were performed in the upper mesosphere/lower thermosphere at Spitsbergen (78°N) in 2001–2003. The cumulative data set covers the season from March until September and altitudes from 80 to 110 km (less in summer). The seasonal variation of K densities shows a maximum from early April until late September, similar to other latitudes but opposite to other metals. Temperatures are derived from the Doppler broadened D1 line of potassium with a typical resolution of 1 km and 1 h, respectively. Systematic temperature uncertainties are approximately ±3 K. Statistical errors depend on integration times and are typically ±0.5–3 K for 1 d and 1 h, respectively. The K-lidar temperatures are generally consistent with simultaneous and colocated in situ measurements by falling spheres. Temperatures show variability on all detectable scales. The magnitude of the fluctuations varies little with season and is remarkably similar to analog observations at lower latitudes (54°N). The summer mesopause is located at ~90 km and is as cold as ~120 K. In winter the mesopause is significantly higher (~100–105 km), warmer (~180–190 K), and less pronounced. Lowest temperatures are detected at the mesopause around 4 July (day of year = 185) which is approximately 2 weeks after astronomical midsummer. Large differences of more than ±20 K occur between mean K temperatures and empirical climatologies. The lower thermosphere is significantly colder compared to general circulation models.

Citation: Höffner, J., and F.-J. Lübken (2007), Potassium lidar temperatures and densities in the mesopause region at Spitsbergen (78°N), *J. Geophys. Res.*, *112*, D20114, doi:10.1029/2007JD008612.

1. Introduction

[2] The upper mesosphere/lower thermosphere (UMLT) is probably the least understood region in the terrestrial atmosphere. This is in part because some important physical processes are fundamentally different here compared to below. For example, infrared radiation is possibly no longer in equilibrium with the trace gases involved (''nonlocal thermodynamic equilibrium,'' non-LTE). The situation is particularly complex at high latitudes during summer where sun light is always present and where global scale dynamics induces temperatures which are some 60–70° below radiative equilibrium. Because this extreme state is sensitive to various physical and chemical processes, e.g., to gravity wave breaking and turbulence, it is well suited to test general circulation models. In addition, various layered phenomena such as noctilucent clouds (NLC) and polar mesosphere summer echoes (PMSE) occur in this height range. These layers critically depend on temperatures in the UMLT and are discussed to be subject of long-term trends [*von Zahn*, 2003; *Thomas et al.*, 2003]. Unfortunately, little is known from observations about the thermodynamic state of the polar summer UMLT since remote measurements of temperatures are challenging and sparse. The main reasons for this deficiency are permanent sunlight which hampers optical observations and non-LTE conditions which can introduce major uncertainties when deriving temperatures from the observed infrared radiation [see, e.g., *Kutepov et al.*, 2006]. In situ techniques such as ''falling spheres'' (FS) have been applied in the past and have resulted in temperature climatologies at several polar latitudes [e.g., *Lübken*, 1999; *Lübken and Müllemann*, 2003]. However, this technique is used sporadically only and barely covers the mesopause region.

[3] In this paper we present potassium lidar (K-lidar) observations of UMLT temperatures from the years 2001 to 2003 performed close to Longyearbyen (78°N, 15°E) on the north polar island Spitsbergen which is part of the archipelago Svalbard. Our mobile K-lidar was transported to Spitsbergen in spring 2001 once it had been developed for daylight capability. Some results regarding NLC, ice particle interaction with potassium atoms, and a comparison with a FS temperature profile have been published in the meantime [*Höffner et al.*, 2003, 2006; *Lübken and Höffner*, 2004]. Here we present a systematic overview of all temperature and potassium density measurements. We will compare our results with the temperature climatology derived from FS measurements performed at the same location in 2001 [*Lübken and Müllemann*, 2003]. We note

[1]Leibniz-Institute of Atmospheric Physics, Kühlungsborn, Germany.

0148-0227/07/2007JD008612$09.00

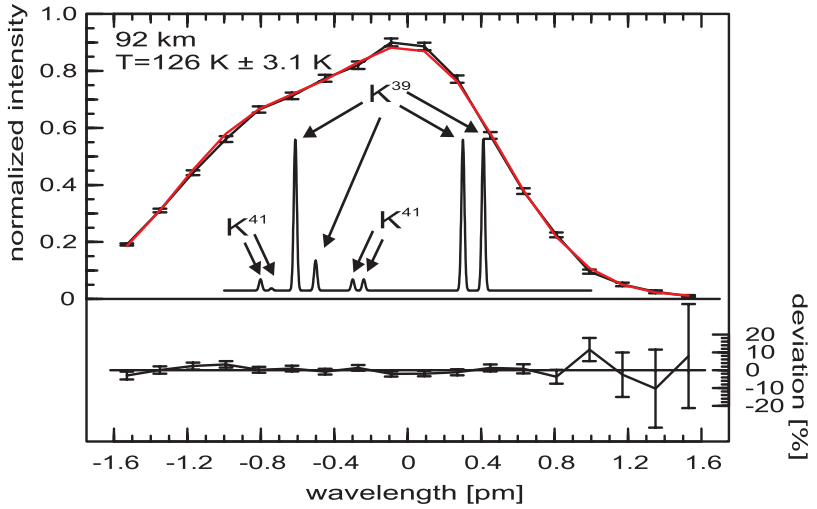

Figure 1. Doppler broadened spectrum of the K resonance lines measured at Spitsbergen on 12 July 2003 from 1930 to 2000 UT at an altitude of 92 ± 1 km. The wavelength axis is relative to the line center at approximately λ = 769.9 nm. The individual lines of the hyperfine structure and their intensities are indicated. The red line shows the fit yielding a temperature of T = 126 ± 3.1 K. In the lower part the relative difference between fit and measured spectrum is shown (in %) including statistical uncertainties.

that our K-lidar observations are unique regarding latitude and height range, accuracy, and temporal and spatial resolution. Beside mean temperatures we also study natural variability. Our observation demonstrate that large variabilities in number densities and temperatures exist at polar latitudes and must be considered in future measurements and models.

2. Experimental Method

2.1. Potassium Lidar

[4] The basic principle to measure temperatures in the upper atmosphere by probing the Doppler broadened line of potassium by the K-lidar has been described by *von Zahn and Höffner* [1996]. Here we present a short overview of the main effects which might influence the temperature retrieval. It turns out that in our case the effects are either not relevant, or can be avoided by careful instrumental design, or can be accounted for in the data analysis. A detailed discussion of all effects is beyond the scope of this paper.

[5] In Figure 1 we show the observed Doppler broadened K(D1) line with statistical uncertainties measured on 12 July 2003 from 1930 to 2000 UT at a solar elevation of 15°, i.e., during full daylight. In Figure 1 we also show the fit of a theoretical line shape which is given by a combination of 8 Voigt functions determined by the individual lifetimes of the corresponding K(D1) transitions of two isotopes. The line shape is further complicated by atomic, atmospheric, and instrumental effects briefly discussed below. Most important the fit considers (1) Doppler broadening (temperature), (2) Doppler shift (vertical wind), (3) amplitude (number density), and (4) a background signal caused by Mie scattering and daylight.

[6] We note that several effects are not important for a potassium lidar but are most likely relevant for resonance lidars based on other species such as sodium or iron. This includes the Hanle effect caused by the Earth's magnetic field, Zeeman and Stark effects, and absorption within the metal layer [*Fricke and von Zahn*, 1985; *Alpers et al.*, 1990; *von Zahn and Höffner*, 1996].

[7] For daylight measurements the field of view (fov) of the telescope and the laser divergence are normally reduced to minimize contamination by solar background radiation. A small laser divergence potentially causes saturation effects, i.e., the backscattered signal is no longer proportional to the laser power [see, e.g., *von der Gathen*, 1991]. To facilitate operation we have used a small fov and laser divergence for all our measurements in all three campaigns, irrespectively of darkness or daylight. Since the saturation effect is wavelength dependent it might result in a temperature bias. *von Zahn and Höffner* [1996] have shown that this effect is small for the K(D1)-line even for strong saturation. We have checked this result at night when the instrument performance does not depend on the field of view. Switching between various configurations (even beyond what is required for daylight measurements) we found no significant influence on the derived temperatures.

[8] The spectral performance of pulsed lasers is a potential source of systematic errors. The finite bandwidth and line shape of the laser broadens the observed spectrum and must be considered. Our laser is a seeded alexandrite ring laser with several improvements compared to commercial lasers. For a reliable spectral performance under field conditions we apply a "ramp and fire" technique to our alexandrite laser, a method which was originally developed for linear Nd:YAG lasers in noisy environments and has recently been applied to satellite instruments [*Henderson et al.*, 1986; *Fry et al.*, 1991; *Nicklaus et al.*, 2007]. Furthermore, in our K-lidar the interference pattern of each single laser pulse is measured with a spectrum analyzer. This information is used to discard laser pulses with bad spectral shape [*von Zahn and Höffner*, 1996]. Finally, the frequency of each laser pulse is measured with a precision of ~1 MHz. The performance and stability of the spectrum analyzer is successfully checked during the field operations in

Spitsbergen by polarization spectroscopy measurements [*Lautenbach*, 2001]. Because the frequency and spectrum of each single laser pulse is measured, technical limitations of pulsed lasers such as frequency jitter, shift in frequency between seeder laser and pulsed laser, or poor spectral performance do not play a role in our case.

[9] For daylight operation a narrow band wavelength filter called FADOF (Faraday Anomalous Dispersion Optical Filter) is installed in the detection system similar to a system applied for sodium since several years [*Chen et al.*, 1996; *Fricke-Begemann et al.*, 2002a; *Höffner and Fricke-Begemann*, 2005]. Since for the potassium D1 transition the transmission is nearly constant over the resonance line there is only a small effect on temperatures (less than 0.5 K). This is not necessarily so for other transitions in potassium or in other gases like sodium. We note that the FADOF also affects the Rayleigh signal which (at stratospheric altitudes) is normally used as a reference and thereby may significantly increase the derived temperatures by up to 10 K. As has been shown by *Höffner and Fricke-Begemann* [2005] we do not need such a reference in our K-lidar and thereby avoid a potential influence of the filter.

[10] Resonance lidar measurements of temperatures rely on accurate intensity measurements at different wavelengths. We use identical optical paths and counting electronics for each individual laser pulse to avoid any bias caused by performance differences. In addition, a complete spectral scan of the resonance line takes less than 1 sec which eliminates the effects of natural variability in tropospheric transmission and K atom number densities.

[11] In summary, the total systematic temperature uncertainty of our K-lidar is estimated to 3 K both for measurements during daylight and darkness. *von Zahn and Höffner* [1996] have earlier estimated an error of 5 K which was mainly caused by an uncertainty in the spectrum analyzer calibration. As mentioned above this uncertainty is significantly reduced by polarization spectroscopy measurements during the field campaigns. As can be seen from Figure 1 there is nice agreement between the measured spectrum and the theoretical fit. Typical relative deviations are less than 1–2% and are randomly distributed, i.e., no systematic deviations are found. This demonstrates the nice performance of the instrument and also confirms that the main physical and instrumental effects are correctly considered in the fit. We continuously control the performance of the K-lidar by permanently monitoring the agreement between measured and fitted spectra. Note that the configuration and performance of the K-lidar was not changed throughout the 3 a being in Spitsbergen.

2.2. Mie Scattering

[12] Around the summer mesopause ice particles are practically permanently present at high latitudes as is known from the permanent occurrence of polar mesosphere summer echoes (PMSE) [*Rüster et al.*, 2001; *Lübken et al.*, 2004b]. If large enough (radii larger than ~10–20 nm) the ice particles may be detected by lidar and are than called "noctilucent clouds" (NLC) [*Hansen et al.*, 1989]. As described in more detail by *Höffner et al.* [2003] we detect a NLC in our spectra as an enhanced signal (relative to the background noise and the air molecule signal) which does not vary when the laser frequency is tuned over the potassium resonance line. We thereby determine scattering from ice particles ("backscatter ratio") and consider their contribution when calculating temperatures. This procedure is particularly important when spectra are averaged over a longer period (for example some hours) since (1) scattering from NLC and potassium atoms may be mixed since both layers may appear at the same altitude at different times (in particular at the lower boundary of the K layer) and (2) "small" ice particles not detectable during short integration may become visible in the spectrum after integration over long periods. We note that ignoring the spectral contribution from ice particles ("large" or "small") in resonance lidar observations may result in substantially too large temperatures (by several tens of Kelvin) since the observed spectrum is effectively broadened. In general the contribution of Mie scattering decreases rapidly with altitude since particle size decreases and Mie scattering depends drastically on particle radius (approximately $\sim r^6$).

2.3. Examples From Winter and Summer

[13] In Figure 2 we show two examples of mean temperature profiles for late winter (16/17 March 2002) and midsummer (25/26 July 2001). The uncertainties shown in these plots result from the fit procedure only, i.e., geophysical variability is not included. The profile from 16/17 March represents a measurement for ~12 h at darkness with relative low K number densities. The uncertainty is less than 2 K between 86 and 108 km because of the long integration time. The profile from 25/26 July represents a daylight measurement for 18 h in the middle of the summer in the presence of Mie scattering. Again the statistical uncertainty is less than 2 K in the entire altitude range. Disadvantages for lidar measurements during summer caused by high solar background and Mie scattering are compensated for by larger potassium number densities The summer maximum is a unique feature of K and different for other metals, e.g., sodium. Still, potassium densities are generally smaller compared to other metals. In both cases shown in Figure 2 the temperature uncertainty is as small as 0.5 K at the peak of the K layer which is negligible compared to natural variability.

[14] Several systematic summer/winter differences are obvious from the profiles shown in Figure 2. The altitude coverage is smaller in summer compared to winter which is caused by daylight conditions, the seasonal variation of K number densities, and the influence of Mie scattering. In summer, measurements concentrate on the height range ~88–97 km, whereas in winter they extend from 85 to 110–115 km. Temperatures in the 88–96 km region are much lower in summer compared to winter. Note that in summer the measured profile differs from the empirical models by more than 20 K (see detailed discussion in section 5).

2.4. Comparison With Falling Spheres

[15] At altitudes below ~90 km we compare the potassium lidar temperatures with falling sphere (FS) measurements. A total of 24 FS were launched between 16 July and 14 September 2001, where four of these launches took place when the K-lidar was in operation [*Lübken and Müllemann*, 2003; *Höffner et al.*, 2003]. The FS technique is published elsewhere [*Schmidlin*, 1991; *Lübken et al.*, 1994]. A mylar

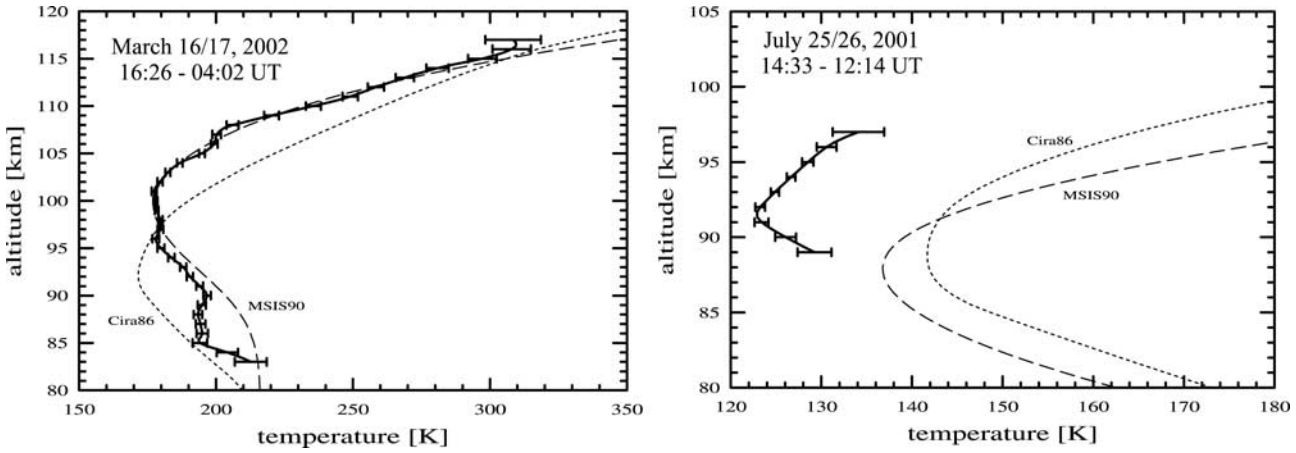

Figure 2. (left) Temperature profile measured in late winter 2002, namely from 16 March, 1626 UT, to 17 March, 0402 UT. The dotted and dashed lines show the corresponding empirical reference profiles for CIRA-86 and MSIS90, respectively. (right) Same for summer 2001, namely from 25 July, 1433 UT, until 26 July, 1214 UT. Note the different scales.

coated plastic sphere is deployed at approximately 110 km and the deceleration is measured by a tracking radar. This technique gives densities and horizontal winds in an altitude range from approximately 95 to 30 km. Temperatures are obtained by integrating the density profile assuming hydrostatic equilibrium. The temperature at the top of the FS profile ("start temperature" T_o) has to be taken from independent measurements or from a model. The seasonal variation of mean temperatures derived from both techniques is very similar (see section 4.1). A first comparison of individual measurements from 28 August 2001 is presented by *Höffner et al.* [2006] and shows nice agreement. A second example from 8 September 2001 is shown in Figure 3. Note that the "start temperature" T_o is taken from the K-lidar which explains the agreement at the top of the FS profile. The gray area in Figure 3 shows the variation of FS temperatures by changing the start temperature by ±10 K. Toward lower altitudes the FS temperatures become more and more independent of T_o. We note that the horizontal distance between the K-lidar and the FS measurements is ∼60 km. Furthermore, the time and altitude resolution of both techniques are rather different. For example, the height resolution of FS at 85 km is only ∼8 km which is significantly less than from the K-lidar. The FS measures a nearly instantaneous profile whereas we have used 1/2 h integration period for the K-lidar profile shown in Figure 3. We have

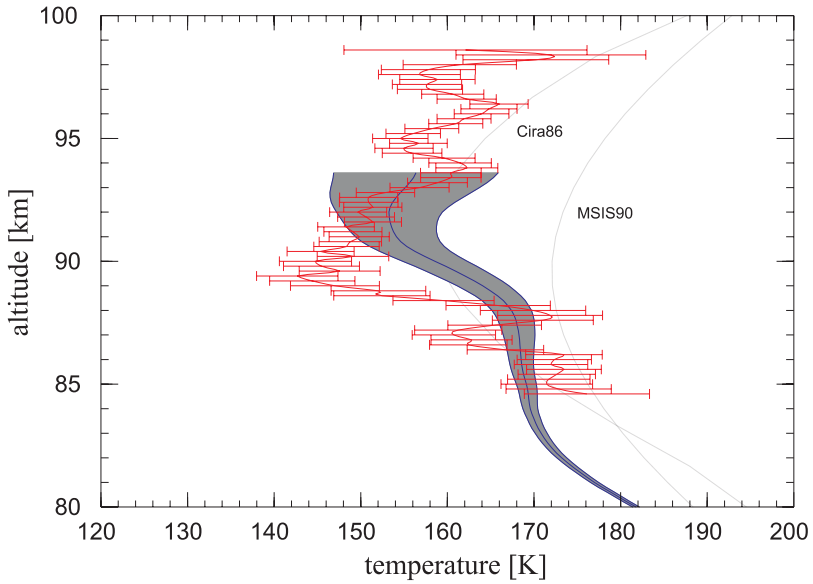

Figure 3. Comparison of temperature profiles from a falling sphere launched on 8 September 2001, 1024 UT (blue line) and K-lidar measurements in the period 1017 to 1045 UT from the same day. The temperature at the top of the FS profile ("start temperature") is taken from the K lidar (see text for more details). The gray area shows the temperature variation if the start temperature is varied by ±10 K. Uncertainties of lidar temperatures are somewhat large because of relatively short integration of only 1/2 h. Reference profiles from CIRA and MSIS-90 are shown for comparison.

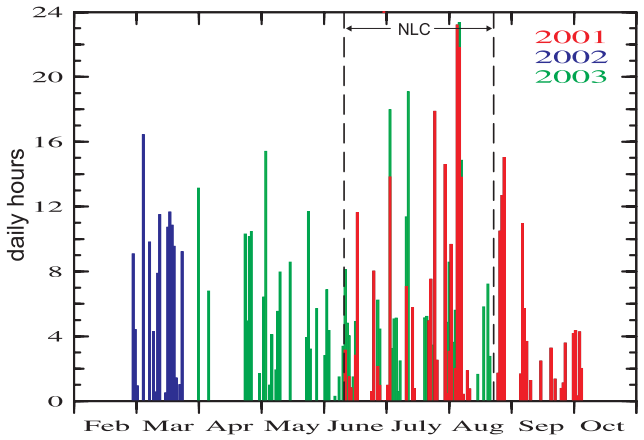

Figure 4. Seasonal variation of the daily hours of K-lidar measurements for the years 2001–2003. Different years are indicated by different colors (see inset). The NLC period is indicated.

tentatively used larger integration periods but the agreement becomes worse because of natural variability. We will present more results on temperature variability from our K-lidar temperatures in section 4.2. Taking into account the differences and limitations of both techniques mentioned above, and natural variability discussed in section 4.2, the agreement between the K-lidar and FS temperature profiles shown in Figure 3 is satisfactory.

2.5. Measurement Statistics

[16] In Figure 4 we show the seasonal coverage of our measurements from 2001 to 2003. A total of 667 h of observations on 120 d are obtained covering the season from 28 February (day of year (DOY) = 59) until 6 October (DOY = 279). The individual periods are listed in Table 1 and the hours available in each month in Table 2. The main emphasis is in summer 2001 and 2003 where most of our lidar measurements took place. Still, the seasonal coverage is fairly complete except for a gap of ~2.5 weeks in April caused by bad weather conditions. The average length of a measurement per day is 5.6 h. Because of unstable weather conditions at Spitsbergen only a few long uninterrupted measurements have been performed. In Figure 5 we show the time of the day of all measurements. In summer the lidar was in operation whenever weather conditions permitted, regardless of the time of day. The two gray areas in Figure 5 indicate a solar elevation of 0° or less. The solar background rises by approximately 3 orders of magnitude when the solar elevation angle increases from approximately −10° to 0° and more. The longest measurement period of 64 h started on 4 August 2001. During summer the entire day is covered by our measurements. In spring the K-lidar was operated during darkness or low solar elevation angles only because K number densities are low at this time of the year (see below). We have marked in Figures 4 and 5 the NLC season, i.e., the period when our lidar detected NLC (12 June to 21 August). A systematic analysis of ice layers (NLC and PMSE) in conjunction with the K-lidar temperature measurements will be published in the near future. We have studied the interannual variation of mean temperatures in summer where measurements from two seasons are available, namely from 2001 and 2003. We find no obvious and systematic differences and therefore decided to take the profiles from all years together when calculating mean K densities, temperatures, and variabilities.

Table 1. Time Periods of Potassium Lidar Measurements in Spitsbergen[a]

Date	Days	Hours
12 Jun to 6 Oct 2001	50	276
28 Feb to 24 Mar 2002	17	120
1 Apr to 21 Aug 2003	53	271

[a]The last two columns give the number of days and the total number of hours with measurements.

3. K Densities

[17] In Figure 6 we show an example of daylight measurements of potassium number densities from 8 September 2001. Densities larger than 10/ccm are shown on a 2 min time and 200 m altitude grid without any further data processing, except background subtraction. Note the strong variability on timescales from ~10 min to several hours. Wavelike features are sometimes visible, for example between approximately 0700 and 1000 UT at 85 and 95 km. As has been shown by *Eska and Höffner* [1998] the response of K densities to gravity waves is mainly due to dynamics, whereas temperature-dependent chemistry effects are comparatively small. On long timescales, however, the variation of K layer is given by meteoric input, ionic and neutral chemistry etc. Waves are acting on this variable background which makes it very difficult to deduce gravity wave parameters from density fluctuations. The variability shown in Figure 6 is typical for most measurements at Spitsbergen and is also found in temperatures (see below) and in NLC [*Lübken and Höffner*, 2004].

[18] The seasonal variation of mean potassium number densities is shown in Figure 7. We have determined the effect of saturation on K density measurements by switching between various fields of view during night, i.e., when solar background is not a problem (see also section 2.1). On the basis of these measurements we have increased the densities by a factor of ~3, independent of season (remember that we have used the same field of view and laser divergence for all campaigns and all seasons). In Figure 7

Table 2. Hours of Potassium Lidar Measurements Available in Each Month

Month	Year	Hours
Jun	2001	32
Jul	2001	75
Aug	2001	118
Sep	2001	36
Oct	2001	15
Feb	2002	9
Mar	2002	111
Apr	2003	56
May	2003	77
Jun	2003	43
Jul	2003	58
Aug	2003	37

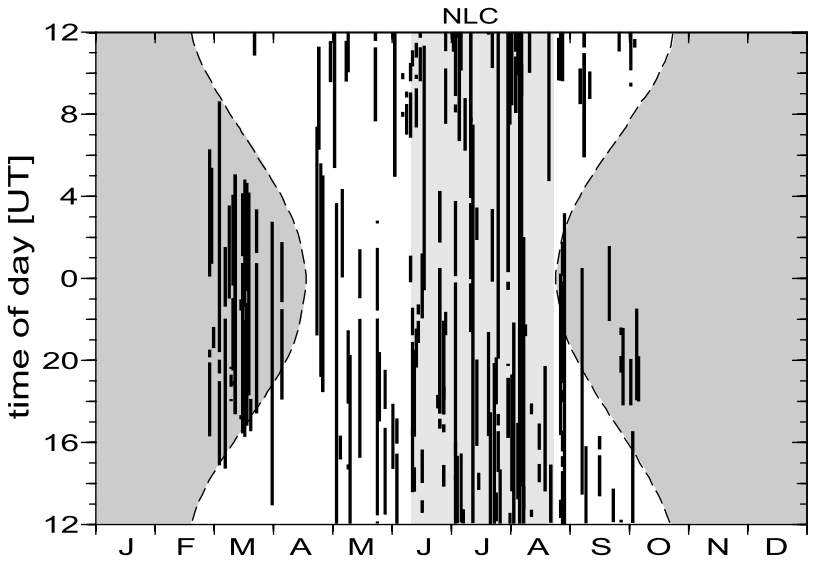

Figure 5. Time-of-day coverage of K-lidar measurements for the years 2001–2003. The two shaded areas in winter correspond to a solar elevation of less then zero degree. The shaded area in summer time indicates the NLC season.

we chose a lower limit of 3/ccm to present the "main layer" introduced by *Höffner and Friedman* [2004]. Smaller number densities exist (in particular at larger altitudes) and can still be detected by our lidar. During darkness the sensitivity of our K-lidar is approximately 0.1/ccm [*Höffner and Friedman*, 2005] which allows temperature measurements up to 115 km. During daylight, number densities of more than 1/ccm are required which limits the height range in summer.

[19] Within the main layer, number densities are smaller in March compared to April–September which points to a seasonal variation opposite to other metals, for example sodium [*She et al.*, 2000]. Furthermore, local maxima of up to ~80/ccm exist at approximately 91–92 km in May and end of August/beginning of September. We have compared our results with similar measurements at lower latitudes, namely at Kühlungsborn (54°N), Tenerife (28°N), and Arecibo (18°N) [*Eska et al.*, 1998; *Höffner and Friedman*, 2004; *Fricke-Begemann et al.*, 2002b; *Friedman et al.*, 2002]. We note that the comparison is limited since data coverage and processing is different at these stations. For example, the K data from Kühlungsborn published by *Eska et al.* [1998] are smoothed by a 90 d filter (compared to 14 d in this paper) which smears out various signatures being important for a detailed comparison. At all four stations potassium densities are generally larger in summer com-

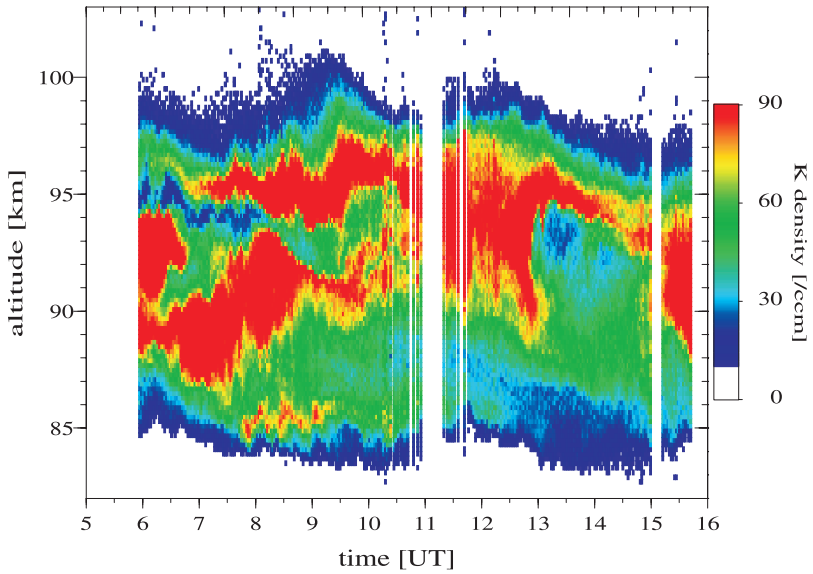

Figure 6. Potassium number densities as a function of altitude and season on 8 September 2001. Note the strong natural variability (typical for Spitsbergen) and wave like features, for example between 0700 and 1000 UT at approximately 85 and 95 km. The data gaps around 1100 UT and 1500 UT are due to bad weather conditions.

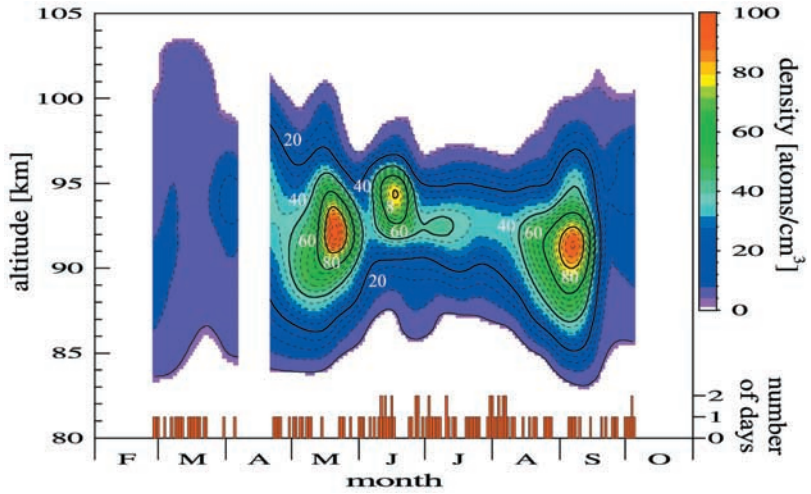

Figure 7. Mean potassium number densities as a function of altitude and season. The color code is given in the plot.

pared to spring and autumn. Maximum mean densities in summer are on the order of 50–100/ccm. The general height structure is again similar, with one major exception namely the lower part of the layer in Spitsbergen. Here the isolines of K densities show an altitude shift from end of March until mid-August. We have demonstrated and quantified earlier that ice particles interact with K atoms and reduce their number densities which explains this effect [*Lübken and Höffner*, 2004; *Raizada et al.*, 2007]. A complete understanding of the seasonal variation of metal densities in the UMLT region requires detailed modeling of sources, sinks, and transport. This is beyond the scope of this paper.

4. Temperatures

4.1. Mean Temperatures

[20] We have summed the photons for each day and determined daily mean temperature profiles by fitting the spectrum as described above. At any given altitude a combination of sinusoidal functions covering yearly (1-y), half-yearly (1/2-y), and quarter-yearly (1/4-y) variations are fitted to these temperatures. An example of temperatures at 90 km and the corresponding fit is shown in Figure 8. The points contributing to the fits are weighted equally because the fluctuations are given by natural variability (nearly independent of season) whereas instrumental errors are much smaller. The average deviation between measurements and fit is ~5 K which demonstrates that the theoretical function introduced above reproduces the mean features of the seasonal variation. As can be seen in Figure 8 we occasionally find larger differences which, however, appear to be random.

[21] In Figure 8 temperatures at 90 km occasionally drop to below 110 K in midsummer and vary rather smoothly in spring and autumn. The fitting procedure demonstrated in Figure 8 was performed at all altitudes and finally results in

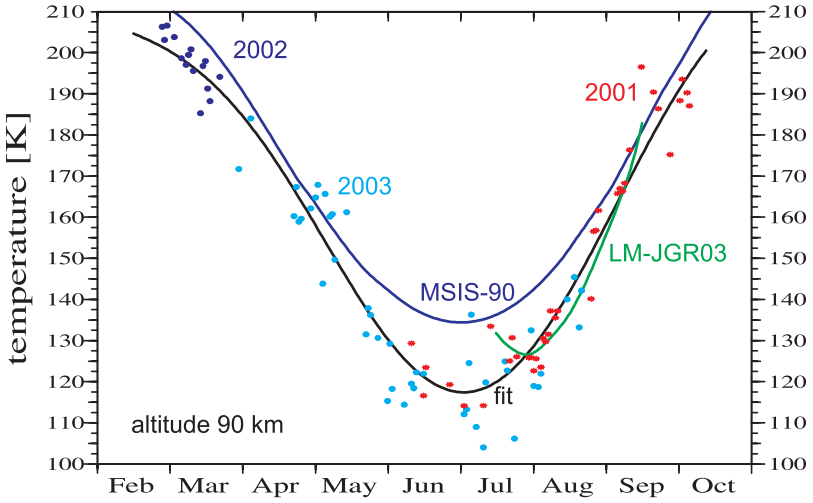

Figure 8. Potassium lidar temperatures at 90 km (dots). Measurements from different years are shown by different colors. The black line shows a sinusoidal fit to the data including a yearly, half-yearly, and quarter-yearly component. For comparison the MSIS-90 empirical reference model (blue) and the FS measurements (green) from *Lübken and Müllemann* [2003] are shown.

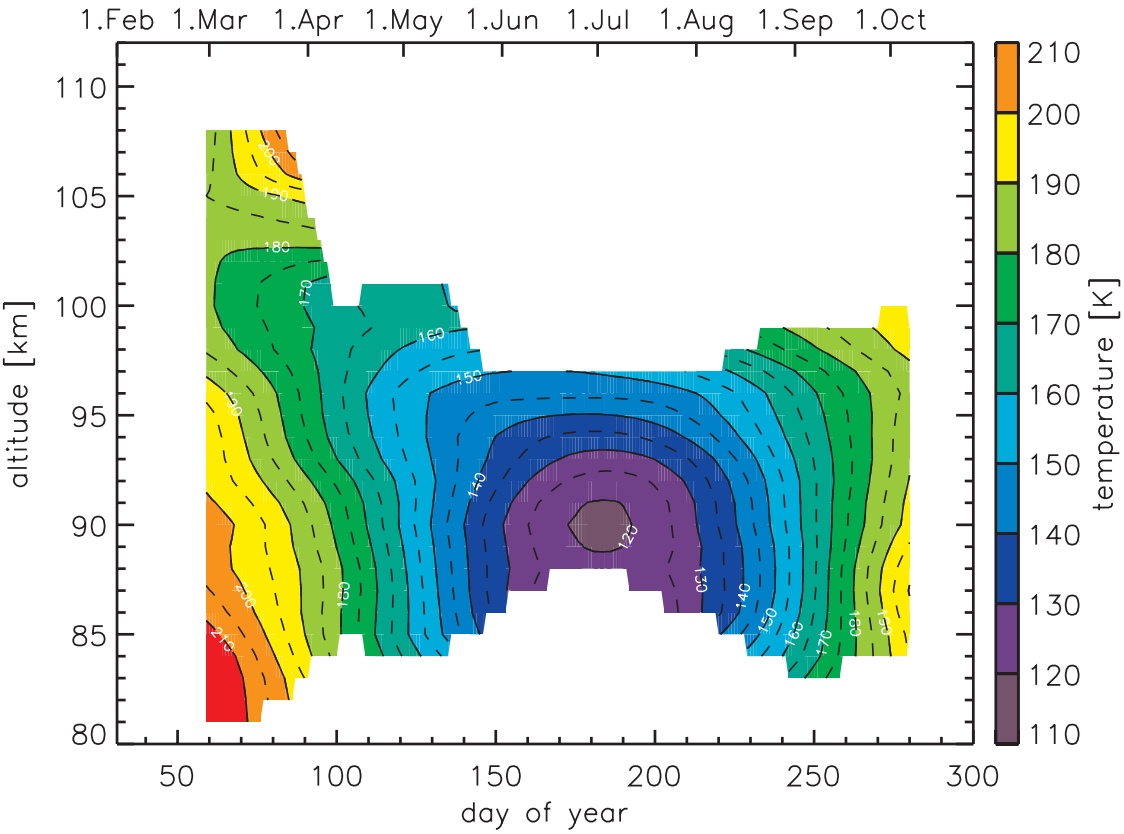

Figure 9. Seasonal variation of mean potassium lidar temperatures.

the mean seasonal variation of the thermal structure in the UMLT region shown in Figure 9 and listed in Table 3. The summer mesopause is located at 90 km and is as cold as 119 K. In winter the mesopause is significantly higher (∼100–105 km), warmer (∼180–190 K), and less pronounced. We note that the atmosphere is nearly isothermal in spring and autumn in the entire height range covered by our lidar. Furthermore, the seasonal variation of temperatures at mesopause altitudes is not symmetric around summer solstice, i.e., it is shifted by ∼14 d toward autumn.

[22] A two-level mesopause in winter/summer has been observed in a global survey by *von Zahn et al.* [1996] and in a compilation of seasonal temperatures at midlatitudes (Fort Collins, 40.6°N, and Kühlungsborn, 54°N) [*She and von Zahn*, 1998]. Our measurements also show the two mesopause levels in "winter" (at ∼100 km) and in summer (at 90 km). In the transition periods the mesosphere is nearly isothermal below ∼95 km, i.e., it is difficult to unambiguously identify a mesopause. Furthermore, our lidar does not really cover the mesopause in the transition region.

[23] The summer mesopause at Spitsbergen (90 km/119 K) is colder and higher compared to lower latitudes. For example, the summer mesopause at 69°N is located at 88 km and is as cold as 129 K [*Lübken*, 1999], i.e., 2 km lower and 10 K warmer compared to Spitsbergen. This trend continues to even lower latitudes, for example 87 km/146 K at 54°N [*Gerding et al.*, 2007] and approximately 86 km/175 K at 40.5°N [*Leblanc et al.*, 1998]. We note that contemporary models like the Leibniz Institute Model of the Atmosphere (LIMA) reflect this cooling and lifting of the mesopause with increasing latitude (U. Berger, Modeling of middle atmosphere dynamics with LIMA, submitted to *Journal of Atmospheric and Solar-Terrestrial Physics*, 2007, hereinafter referred to as Berger et al., submitted manuscript, 2007).

[24] In Figure 10 we show amplitudes and phases of the sinusoidal fits mentioned above. The phase is defined as the date when temperatures reach a minimum.

[25] We concentrate on altitudes where reliable data for the entire period are available (88–96 km). The 1-y component is largest at all heights with typical amplitudes of 40–50 K, slightly decreasing with altitude. This corresponds to a peak-to-peak variation of nearly 100 K throughout the season. The 1/2-y component is much smaller with an amplitude of ∼12–14 K at 89–91 km rapidly decreasing above. The 1/4-y amplitude is generally less than 4 K. We have tentatively fitted a 1-y component only but systematic deviations occurred and the main features of the seasonal variation were not covered satisfactorily. It is interesting to note that the 1-y and 1/2-y amplitudes are largest around the height of the summer mesopause. The combination of 1-y and 1/2-y amplitudes and phases results in the coldest day on 4 July (DOY = 185), i.e., 13 d after summer solstice. We do not show phases at altitudes where the amplitudes are very small since uncertainties are too large (e.g., for the 1/2-y component above 93 km). At 90 km, for example, the 1-y and 1/2-y phases differ significantly which corresponds to the nonsymmetric (around midsummer) temperature variation. Indeed, the maximum temperature gradients in the transition periods, namely at the beginning of May (−1.0 K/d) and at

Table 3. Mean Temperatures in Kelvin From Potassium Lidar

	DOY																						
km	60	70	80	90	100	110	120	130	140	150	160	170	180	190	200	210	220	230	240	250	260	270	280
108	183	194	204																				
107	184	192	201																				
106	184	191	197																				
105	185	187	189	192																			
104	183	184	185	187																			
103	181	181	182	183																			
102	181	179	177	175																			
101	181	177	174	170		164	162	160															
100	181	177	173	170	167	164	162	161															
99	182	178	174	171	168	165	163	162	160										180	184	187	191	194
98	184	180	175	171	167	163	160	158	156									171	175	179	184	188	192
97	188	183	178	172	167	162	157	154	152	150	150	150	150	151	153	155	159	163	168	173	179	184	188
96	193	187	181	174	166	159	154	150	148	147	146	146	146	147	147	149	152	157	163	169	176	181	187
95	196	189	182	174	167	160	154	149	146	143	141	140	140	140	142	145	150	155	161	168	175	181	188
94	198	191	183	175	168	161	155	149	144	140	137	134	133	134	136	140	146	152	159	167	174	181	189
93	198	192	185	178	170	163	156	150	144	139	134	130	128	128	130	135	141	149	157	165	173	181	189
92	198	194	188	181	174	166	159	151	143	136	130	126	123	123	126	131	138	146	155	164	173	182	190
91	201	197	191	185	177	169	160	150	141	133	127	122	120	120	123	128	136	145	154	164	174	183	191
90	203	199	194	187	179	169	160	150	140	132	125	121	119	119	123	128	135	144	154	164	175	184	192
89	202	199	194	188	180	171	161	151	141	132	126	122	120	120	123	127	134	143	153	164	175	186	196
88	203	199	195	189	182	172	162	151	141	133	127	123	121	122	124	128	134	142	152	164	177	189	199
87	205	201	195	189	182	173	163	152	142	133	126				122	127	134	142	153	164	177	189	200
86	208	203	196	189	181	172	163	153	143	133						127	134	143	154	165	177	188	199
85	212	205	198	190	181	172	162	153	144								140	148	157	167	177	187	196
84	216	209	201	192	183	174	165	157										153	160	168	177	186	
83	218	211	203	195																172			
82	218	211	204																				
81	218	211																					

the end of August (1.1 K/d), are different. We note that an asymmetry in the transition periods is also observed at lower latitudes (50–60°N) but the difference is significantly larger compared to Spitsbergen [see *Shepherd et al.*, 2004, Figure 4]. At these lower latitudes the transition at 87 km is much faster (in magnitude) in spring (∼−0.76 K/d) compared to autumn (∼+0.42 K/d).

4.2. Variability on Short Timescales

[26] We have studied the natural variability of temperatures on short timescales by comparing actual measurements with a mean for a period of approximately 1 d. In Figure 11 this deviation is shown for a period of 10 h on 8 September 2001. Temperatures were calculated for time and height bins of 15 min and 1 km, shifted by increments of 5 min and 200 m, respectively. The short integration time results in somewhat large uncertainties of approximately 5 K. In Figure 11 a downward progressing wave front is clearly visible with an amplitude exceeding 30 K. On top of this wave some further variability is detected down to the smallest temporal scales available. As can be seen from Figure 11 the FS launch discussed in section 2.4 took place in a period of very low temperatures caused by a wave with a period of roughly 4 h.

[27] Following *Rauthe et al.* [2006] we have characterized the temperature fluctuations as follows. At any given altitude we determine the fluctuations (=actual measurement minus daily mean) on a single day and then calculate the mean and the standard deviation of the fluctuations from all days available in a given month. The fluctuations on a single day are determined from hourly mean profiles but only if at least 3 h are available and only if the statistical uncertainty is less then 10 K (such a large error limit is only relevant at the upper/lower boundary of the K layer). The results of our analysis are shown in Figure 12 for March in Spitsbergen (11 d) and Kühlungsborn (21 d). Similar results are shown for July (16 d in Spitsbergen and 46 d in Kühlungsborn). The statistical uncertainty (''noise'') of our measurements is typically 3–5 K This corresponds to mean fluctuations of less then 1 K which is much smaller then the ''signal'' of 6–10 K shown in Figure 12. This is true for both stations. In March the mean fluctuations increase with altitude from ∼6 K at 86 km to ∼10 K at 103 km at both locations. A similar increase is observed in July, but the height coverage in Spitsbergen is comparatively small.

[28] The magnitudes of the mean fluctuations are rather similar at 78° and 54°, respectively. This is surprising because the thermal structure in the mesosphere is rather different at both locations. A given gravity wave, for example, would therefore create rather different fluctuations at both places. We note that the mean fluctuations are similar in all months available. Examples for March and July are presented in Figure 12. Some differences occur but they are rather small compared to the variability of the mean. This result is remarkable since most models predict a rather strong seasonal variation of wave activity in the upper atmosphere caused by differences in wave generation, filtering, and breaking [see, e.g., *Lindzen*, 1981; *Garcia and Solomon*, 1985; *Schmidt et al.*, 2006].

[29] A comprehensive comparison of measured and modeled variabilities at various stations requires considerations

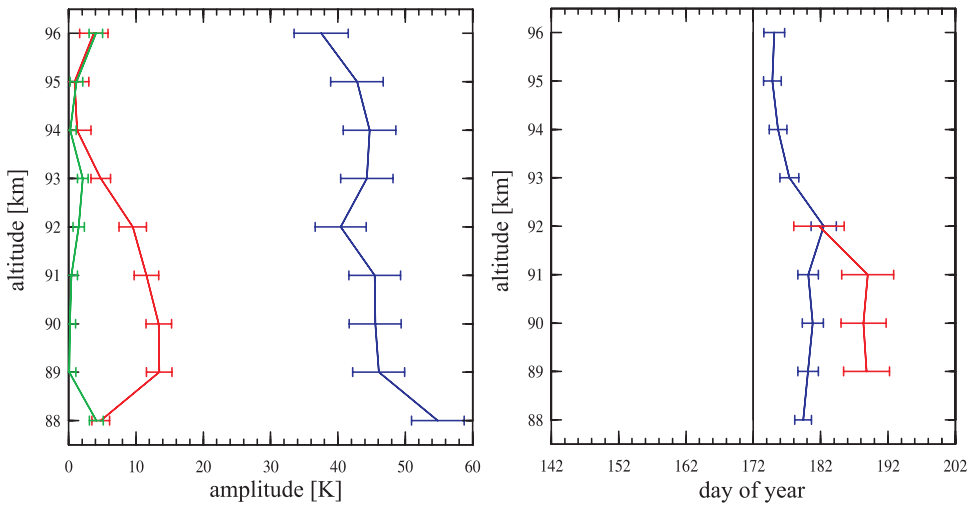

Figure 10. Amplitudes and phases of sinusoidal components of potassium temperatures with periods of 1 a (blue), 1/2 a (red), and 1/4 a (green). Astronomical midsummer (21 June) corresponds to day-of-year = 172. The phase is defined as the date when temperatures reach a minimum. The phase for the 1/4 y component is not shown since it is not significant because of too small amplitudes.

of the thermal and dynamical background, and a spectral characterization of the fluctuations. This is beyond the scope of this paper.

5. Comparison With Measurements and Reference Atmospheres

[30] Little is known about the thermal structure in the UMLT region at high latitudes, in particular in summer (one of the main focus of this paper). Summer climatologies based on falling sphere data have been published for Andøya (69°N) and Rothera (68°S) but this technique barely covers the mesopause [*Lübken*, 1999; *Lübken et al.*, 2004a]. *Pan and Gardner* [2003] have summarized their lidar measurements at the South Pole but only 26 h of Fe lidar temperatures are available in the 4 summer months (November–February), compared to 440 h in the period May–August in this paper. Furthermore, none of the South Pole summer profiles covers the mesopause.

[31] We have earlier mentioned the FS campaign performed at Spitsbergen in 2001. Our lidar temperatures generally agree with the FS climatology at Spitsbergen published by *Lübken and Müllemann* [2003, Figure 8; see also *Höffner et al.*, 2006, Figures 1 and 2]. There is one exception, namely in mid-July around 90 km where FS temperatures observed in 2001 are typically 10 K higher compared to the mean lidar temperatures from 2001 and 2003 (see Figure 8). We have studied this difference in detail and found from our lidar data that temperatures in mid-July 2001 are indeed larger compared to 2003, i.e., the difference is due to geophysical variability. It should be noted that 90 km is close to the upper height limit of the

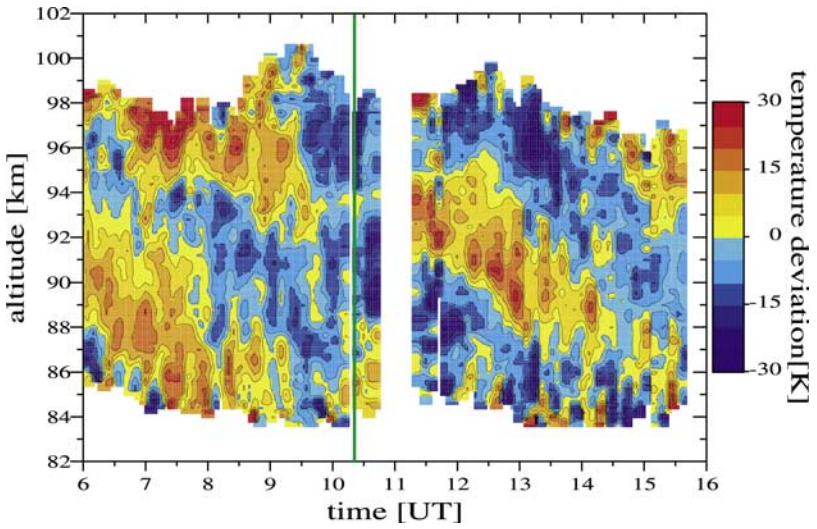

Figure 11. Temperature deviations relative to a daily mean for a period of ~10 h on 8 September 2001. Variations of up to ±30 K are present (see color bar). The vertical line at 1024 UT indicates the launch of a falling sphere.

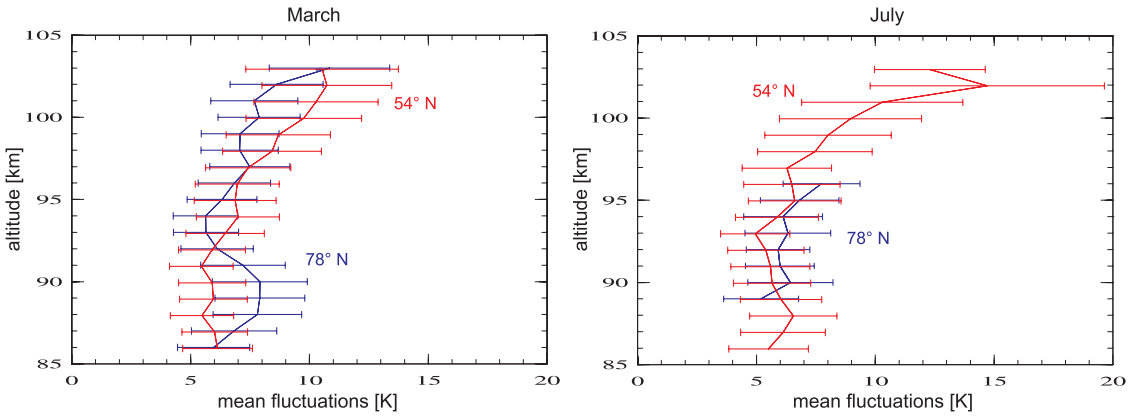

Figure 12. Mean of daily temperature fluctuations in (left) March and (right) July at Spitsbergen (78°N, blue) and Kühlungsborn (54°N, red). The variability of the mean fluctuations is also shown (horizontal bars).

falling sphere technique, and, furthermore, only few flights contribute to the FS mean in mid-July 2001 (see *Lübken and Müllemann* [2003] for more details). From Figure 8 we also see that temperatures in midsummer (end of June/beginning of July) are significantly lower compared to end of July. This implies that the field campaign providing data for the FS climatology started too late to cover the lowest summer mesopause temperatures.

[32] There are systematic and large differences of our summer temperatures compared to empirical reference models such as CIRA-1986 (COSPAR international reference atmosphere) and MSIS (mass spectrometer and incoherent scatter data) [*Fleming et al.*, 1990; *Hedin*, 1991]. We compare our results with two versions of MSIS, namely from 1990 and from 2000 which are labeled "MSIS-90" and "MSIS-00" hereafter [*Hedin*, 1991; *Picone et al.*, 2002].

[33] In Figure 13 we show differences of our mean lidar temperatures to CIRA-1986. Negative values indicate that the K-lidar results are colder compared to CIRA. Large differences ranging from −30 to +20°K occur. The summer mesopause is too warm and too low in CIRA compared to measurements (see also Figure 2). In midsummer the K-lidar mesopause is located at 90 km with a temperature of 119 K, whereas in CIRA the mesopause is at the same altitude but with a temperature of 139 K. In spring, CIRA is too cold by more than 20 K at altitudes around 90 km and too warm by similar amounts above ∼100 km. This implies that the mean temperature gradient in the lower thermosphere is smaller in our measurements compared to CIRA

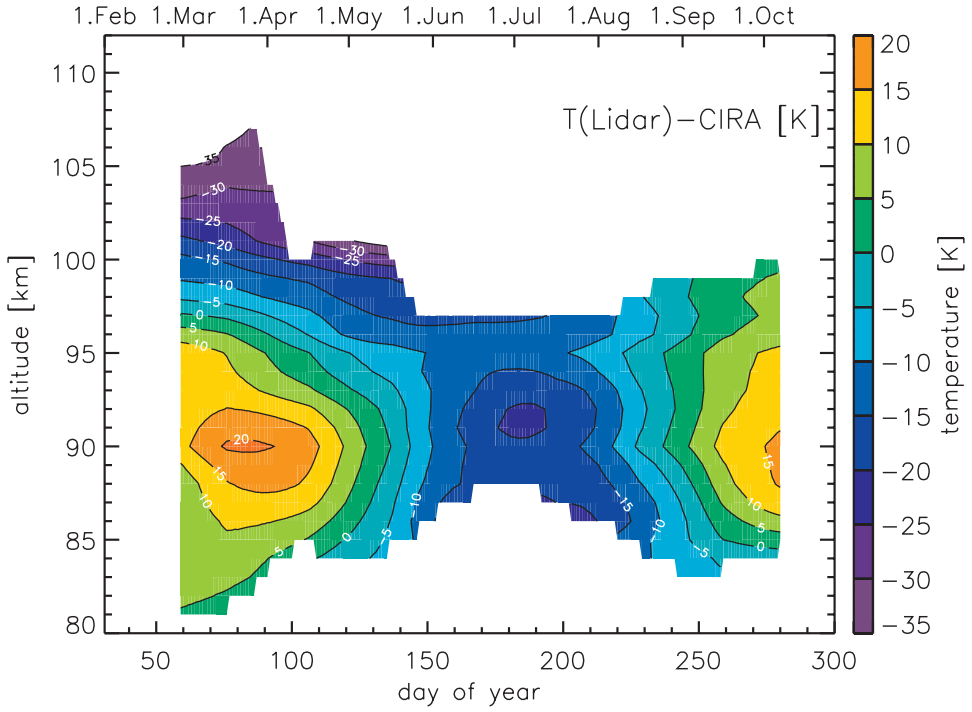

Figure 13. K-lidar temperatures minus CIRA-86. Blue colors indicate that lidar temperatures are lower compared to CIRA-86.

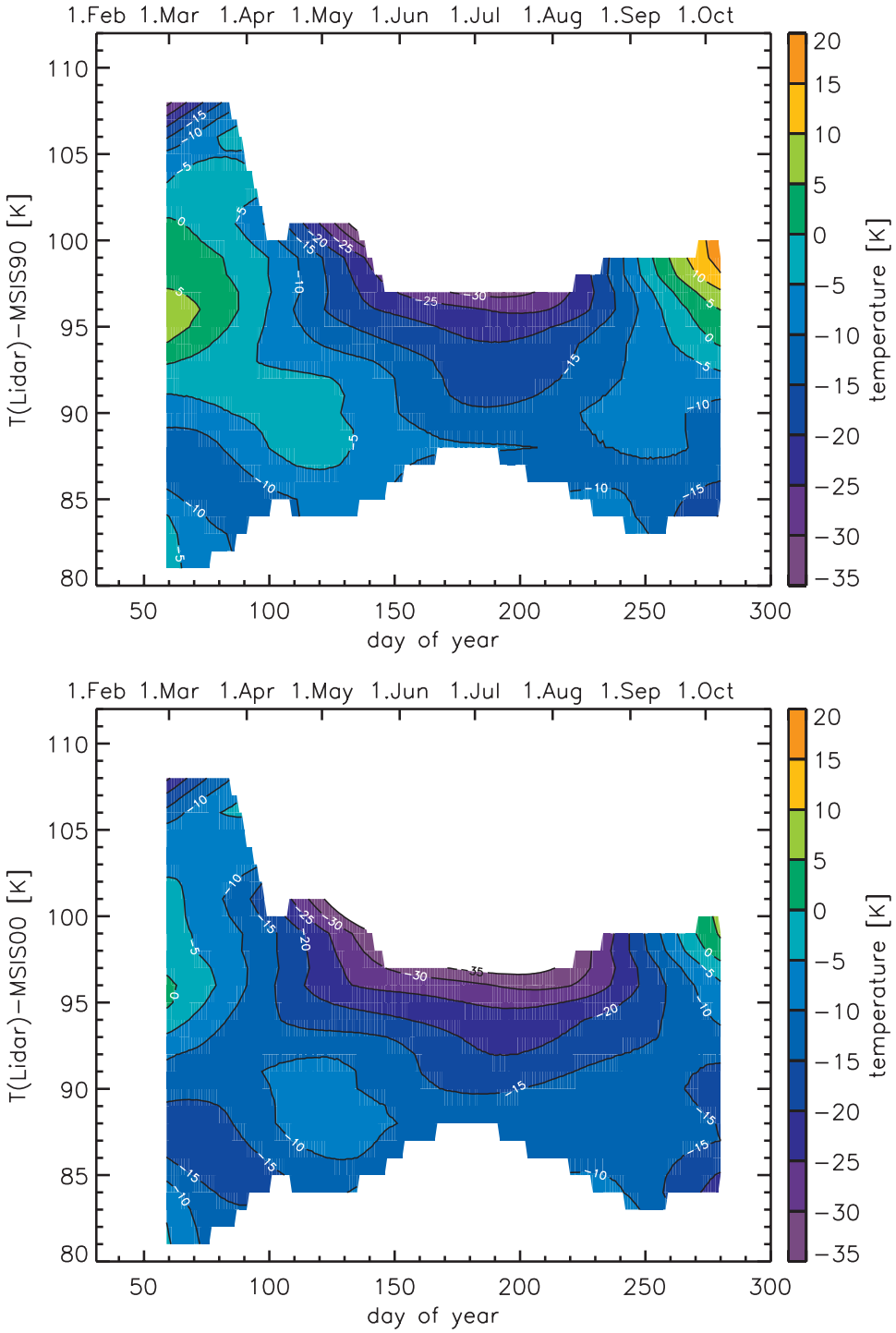

Figure 14. K-lidar temperatures minus (top) MSIS-90 and (bottom) MSIS-00. Blue colors indicate that lidar temperatures are lower compared to MSIS.

by as much as ∼50 K/15 km. Such a large difference is important for static stability, but also for the temperature retrieval from meteor radars [see *Hall et al.*, 2004, and references therein]. CIRA does not satisfactorily reproduce the fast transition of the thermal structure at mesopause altitudes in spring and autumn. *Leblanc et al.* [1998] have studied temperature differences of lidar climatologies at midlatitudes relative to CIRA-1986. They also find large discrepancies (up to 20 K and more) but the seasonal variation of the differences is quite different compared to our results. At ∼90 km the differences are rather uniform at midlatitudes, whereas at Spitsbergen they vary from +20 K in spring and autumn to −20 K in summer.

[34] In Figure 14 we show differences to the two latest versions of MSIS introduced above. Both versions of MSIS are generally too warm by 10 to 20 K, nearly independent of season and altitude. The difference between the two versions of MSIS is small compared to the deviations from our

observations. The MSIS-00 mesopause in midsummer (DOY = 182) is at 88 km with a temperature of 132 K, which is too low and too warm compared to our measurements. This implies that the lower thermosphere is colder than in MSIS by up to 30 K. This has important implications for ice particle nucleation and morphology. In spring and in the height range ~90–105 km there is general agreement between our measurements and MSIS-90 and MSIS-00.

[35] As has been shown earlier the general appearance of noctilucent clouds and polar mesosphere summer echoes at Spitsbergen is consistent with the occurrence of supersaturated atmospheric regions [*Höffner et al.*, 2003; *Lübken et al.*, 2004b]. Since the degree of saturation is very sensitive to atmospheric temperatures this nicely confirms the accuracy of our lidar temperature measurements. Certainly, the reference model temperatures presented above are not consistent with NLC and PMSE.

[36] We note that some general circulation models are nowadays available to reproduce the very cold summer upper mesosphere [see, e.g., *Berger and von Zahn*, 1999; *Schmidt et al.*, 2006; Berger et al., submitted manuscript, 2007]. Still, compared to our K-lidar observations major differences by more than 10 K and up to 5 km exist for mesopause temperatures and altitudes, respectively. In addition, the temperature gradient directly above the mesopause is generally smaller in our lidar data compared to models. As a consequence of these differences the lowermost thermosphere is much colder in our observations by more than 30 K compared to models. As we demonstrate in a companion paper this difference has significant consequences for the appearance of PMSE (F.-J. Lübken et al., Lidar temperatures, nocticulent clouds, and polar mesosphere summer echoes at Spitsbergen (78°N), manuscript in preparation, 2007). It remains to be seen which physical process is responsible for this discrepancies.

[37] We have not compared our results with satellite temperature measurements, for example from the SABER instrument on TIMED since optical infrared techniques suffer from the large solar background and from several uncertainties introduced by non-LTE conditions at the summer mesopause and above [*Kutepov et al.*, 2006].

6. Conclusion

[38] Lidar measurements of potassium temperatures and number densities were performed in the upper mesosphere/lower thermosphere (UMLT) at Spitsbergen in the years 2001–2003. The cumulative data set covers the season from March to September. These data present the first comprehensive probing of potassium densities and atmospheric temperatures at Arctic polar latitudes. The seasonal variation of K densities shows a maximum around 90–95 km from early April until late September, opposite to the variation observed for other metals at lower latitudes.

[39] Temperatures are derived from the Doppler broadened D1 line of potassium. A theoretical spectrum is fitted to the measured spectrum taking into account instrumental and atmospheric properties. The agreement between the fit and the measured spectrum is continuously checked. Atmospheric temperatures, potassium densities, Mie scattering from ice particles, etc. are derived from the fit. Theoretical fits nicely agree with measured spectra where the deviations are less than 1–2% and are randomly distributed. The quality of each single laser pulse is controlled by means of a spectrum analyzer. The temperature error due to systematic instrumental effects is approximately ±3 K, independent of operation during day or night. Temperature uncertainties due to photon statistics depend on, for example, integration time and potassium densities. Under good conditions a typical temporal and spatial resolution is 1 km and 15 min and gives temperatures with an uncertainty of less than 5 K, both for operation under daylight and during darkness. For a height bin of 1 km and typical potassium densities, statistical uncertainties are 1–3 K and <1 K when integrating the signal for 1 h and 1 d, respectively. This is considerably less than typical natural variability. The altitude coverage is larger in spring/autumn compared to summer because of seasonal variation of photon noise and K densities. Temperatures from our K-lidar are consistent with in situ measurements performed by falling spheres from mid-July to mid-August 2001. The agreement is satisfactory both for single flights and for the mean seasonal variation.

[40] The K-lidar temperature profiles show variability on all detectable scales. Temperature variabilities on an hourly basis are surprisingly similar to analog observations at Kühlungsborn (54°N). Fluctuations generally increase with height but show little variation with season. Our measurements show that the summer mesopause is located at ~90 km and is as cold as ~120 K. In winter the mesopause is significantly higher (~100–105 km), warmer (~180–190 K), and less pronounced. In the transition periods, more precisely in beginning of April and in mid-September, the UMLT is nearly isothermal with temperatures close to 180 K. Lowest temperatures are detected at the mesopause around 4 July (DOY = 185) which is approximately 2 weeks after astronomical midsummer (21 June = DOY 172). At 90 km the seasonal variation is slightly asymmetric in time (around midsummer) where the asymmetry is smaller at higher altitudes. Large differences of more than ±20 K exist between mean K temperatures and the CIRA empirical climatology. In particular, the summer mesopause is up to 20 K colder compared to CIRA. In winter mean temperature gradients in the UMLT derived from our K lidar differ from CIRA by more than 50 K/15 km. MSIS is generally too warm where the largest differences appear in the summer lower thermosphere. We have tentatively compared our temperature measurements with GCM models. Differences are most obvious in summer at the mesopause and in the lower thermosphere, both regions being generally too warm in the models.

[41] **Acknowledgments.** We thank Jens Lautenbach for his assistance in performing the K-lidar measurements in Spitsbergen and processing and analyzing the data. The field measurements were further supported by C. Fricke-Begemann, P. Keller, T. Köpnick, J. Liu, and P. Menzel. This research is supported by the Deutsche Forschungsgemeinschaft (DFG) under the CAWSES SPP grant LU 1174/3-1 (SOLEIL) and by the German Space Agency (DLR) under grant 50 OE 9901 (ROMA).

References

Alpers, M., J. Höffner, and U. von Zahn (1990), Iron atom densities in the polar mesosphere from lidar observations, *Geophys. Res. Lett.*, *17*, 2345–2348.

Berger, U., and U. von Zahn (1999), The two-level structure of the mesopause: A model study, *J. Geophys. Res.*, *104*, 22,083–22,093.
Chen, H., M. A. White, D. A. Krueger, and C. Y. She (1996), Daytime mesopause temperature measurements with a sodium-vapor dispersive Faraday filter in a lidar receiver, *Opt. Lett.*, *21*, 1093–1095.
Eska, V., and J. Höffner (1998), Observed linear and nonlinear K layer response, *Geophys. Res. Lett.*, *25*, 2933–2936.
Eska, V., J. Höffner, and U. von Zahn (1998), Upper atmosphere potassium layer and its seasonal variations at 54°N, *J. Geophys. Res.*, *103*(A12), 29,207–29,214.
Fleming, E. L., S. Chandra, J. J. Barnett, and M. Corney (1990), Zonal mean temperature, pressure, zonal wind, and geopotential height as functions of latitude, *Adv. Space Res.*, *10*(12), 11–59.
Fricke, K., and U. von Zahn (1985), Mesopause temperatures derived from probing the hyperfine structure of the D2 resonance line of sodium by lidar, *J. Atmos. Terr. Phys.*, *47*, 499–512.
Fricke-Begemann, C., M. Alpers, and J. Höffner (2002a), Daylight rejection with a new receiver for potassium resonance temperature lidars, *Opt. Lett.*, *27*(21), 1932–1934.
Fricke-Begemann, C., J. Höffner, and U. von Zahn (2002b), The potassium density and temperature structure in the mesopause region (80–105 km) at a low latitude (28°N), *Geophys. Res. Lett.*, *29*(22), 2067, doi:10.1029/2002GL015578.
Friedman, J. S., S. C. Collins, R. Delgado, and P. A. Castleberg (2002), Mesospheric potassium layer over the Arecibo observatory, 18.3°N 66.75°W, *Geophys. Res. Lett.*, *29*(5), 1071, doi:10.1029/2001GL013542.
Fry, E. S., Q. Hu, and X. Li (1991), Single-frequency operation of an injection-seeded Nd:YAG laser in high noise and vibration environments, *Appl. Opt.*, *30*(9), 1015–1017.
Garcia, R. R., and S. Solomon (1985), The effect of breaking gravity waves on the dynamics and chemical composition of the mesosphere and lower thermosphere, *J. Geophys. Res.*, *90*, 3850–3868.
Gerding, M., J. Höffner, M. Rauthe, W. Singer, M. Zecha, and F.-J. Lübken (2007), Simultaneous observation of NLC, MSE and temperature at a mid-latitude station 54°N, *J. Geophys. Res.*, *112*, D12111, doi:10.1029/2006JD008135.
Hall, C., T. Aso, M. Tsutsumi, J. Höffner, and J. Sigernes (2004), Multi-instrument derivation of 90 km temperatures over Svalbard (78°N, 6°E), *Radio Sci.*, *39*, RS6001, doi:10.1029/2004RS003069.
Hansen, G., M. Serwazi, and U. von Zahn (1989), First detection of a noctilucent cloud by lidar, *Geophys. Res. Lett.*, *16*, 1445–1448.
Hedin, A. E. (1991), Extension of the MSIS thermosphere model into the middle and lower atmosphere, *J. Geophys. Res.*, *96*, 1159–1172.
Henderson, S. W., E. H. Yuen, and E. S. Fry (1986), Fast resonance-detection technique for single-frequency operation of injection-seeded Nd:YAG lasers, *Opt. Lett.*, *11*(11), 715–717.
Höffner, J., and C. Fricke-Begemann (2005), Accurate lidar temperatures with narrowband filters, *Opt. Lett.*, *30*(8), 890–892.
Höffner, J., and J. S. Friedman (2004), The mesospheric metal layer topside: A possible connection to meteoroids, *Atmos. Chem. Phys.*, *4*, 801–808.
Höffner, J., and J. S. Friedman (2005), The mesospheric metal layer topside: Examples of simultaneous metal observations, *J. Atmos. Sol. Terr. Phys.*, *67*, 1226–1237, doi:10.1016/j.jastp.2005.06.010.
Höffner, J., C. Fricke-Begemann, and F.-J. Lübken (2003), First observations of noctilucent clouds by lidar at Svalbard, 78°N, *Atmos. Chem. Phys.*, *3*, 1101–1111.
Höffner, J., J. Lautenbach, C. Fricke-Begemann, and F.-J. Lübken (2006), Polar mesosphere temperature observations by lidar and falling sphere at 78°N, in *Proceedings of the 23rd ILRC Conference, Nara, Japan, 24–28 July 2006*, edited by C. Nagasawa, and N. Sugimoto, pp. 373–376, Conf. Steering Comm. of the 23rd Int. Laser Radar Conf., Nara, Japan.
Kutepov, A. A., A. G. Feofilov, B. T. Marshall, L. L. Gordley, W. D. Pesnell, R. A. Goldberg, and J. M. Russell III (2006), SABER temperature observations in the summer polar mesosphere and lower thermosphere: Importance of accounting for the CO_2 ν_2 quanta VV exchange, *Geophys. Res. Lett.*, *33*, L21809, doi:10.1029/2006GL026591.
Lautenbach, J. (2001), Aufbau einer Doppler-freien Polarisationsspektroskopie als Wellenlängenstandard anhand der Kalium (D1)-Linie, Master's thesis, Tech. Fachhochsch., Wildau, Germany.
Leblanc, T., I. S. McDermid, P. Keckhut, A. Hauchecorne, C. She, and D. A. Krueger (1998), Temperature climatology of the middle atmosphere from long-term lidar measurements at middle and low latitudes, *J. Geophys. Res.*, *103*, 17,191–17,204.
Lindzen, R. S. (1981), Turbulence and stress owing to gravity wave and tidal breakdown, *J. Geophys. Res.*, *86*, 9707–9714.
Lübken, F.-J. (1999), Thermal structure of the Arctic summer mesosphere, *J. Geophys. Res.*, *104*, 9135–9149.
Lübken, F.-J., and J. Höffner (2004), Experimental evidence for ice particle interaction with metal atoms at the high latitude summer mesopause region, *Geophys. Res. Lett.*, *31*, L08103, doi:10.1029/2004GL019586.
Lübken, F.-J., and A. Müllemann (2003), First in situ temperature measurements in the summer mesosphere at very high latitudes (78°N), *J. Geophys. Res.*, *108*(D8), 8448, doi:10.1029/2002JD002414.
Lübken, F.-J., et al. (1994), Intercomparison of density and temperature profiles obtained by lidar, ionization gauges, falling spheres, datasondes, and radiosondes during the DYANA campaign, *J. Atmos. Terr. Phys.*, *56*, 1969–1984.
Lübken, F.-J., A. Müllemann, and M. J. Jarvis (2004a), Temperatures and horizontal winds in the Antarctic summer mesosphere, *J. Geophys. Res.*, *109*, D24112, doi:10.1029/2004JD005133.
Lübken, F.-J., M. Zecha, J. Höffner, and J. Röttger (2004b), Temperatures, polar mesosphere summer echoes, and noctilucent clouds over Spitsbergen (78°N), *J. Geophys. Res.*, *109*, D11203, doi:10.1029/2003JD004247.
Nicklaus, K., V. Morasch, M. Höfer, J. Luttmann, M. Vierkoetter, H.-D. Hoffmann, M. Ostermeyer, and J. Höffner (2007), Frequency stabilisation of q-switched Nd:YAG oscillators for airborne and spaceborne LIDAR systems, *Proc. SPIE Int. Soc. Opt. Eng.*, *6451*, 64511L-1-12.
Pan, W., and C. S. Gardner (2003), Seasonal variations of the atmospheric temperature structure at South Pole, *J. Geophys. Res.*, *108*(D18), 4564, doi:10.1029/2002JD003217.
Picone, J. M., A. E. Hedin, D. P. Drob, and A. C. Aikin (2002), NRL-MSISE-00 empirical model of the atmosphere: Statistical comparison and scientific issues, *J. Geophys. Res.*, *107*(A12), 1468, doi:10.1029/2002JA009430.
Raizada, S., M. Rapp, F.-J. Lübken, J. Höffner, M. Zecha, and J. M. C. Plane (2007), The effect of ice particles on the mesospheric potassium layer at Spitsbergen 78°N, *J. Geophys. Res.*, *112*, D08307, doi:10.1029/2005JD006938.
Rauthe, M., M. Gerding, J. Höffner, and F.-J. Lübken (2006), Lidar measurements of temperature gravity waves over Kühlungsborn 54°N from 1–105 km: A winter-summer comparison, *J. Geophys. Res.*, *111*, D24104, doi:10.1029/2006JD007354.
Rüster, R., J. Röttger, G. Schmidt, P. Czechowsky, and J. Klostermeyer (2001), Observations of mesospheric summer echos at VHF in the polar cap region, *Geophys. Res. Lett.*, *28*, 1471–1474.
Schmidlin, F. J. (1991), The inflatable sphere: A technique for the accurate measurement of middle atmosphere temperatures, *J. Geophys. Res.*, *96*, 22,673–22,682.
Schmidt, H., et al. (2006), The HAMMONIA chemistry climate model: Sensitivity of the mesopause region to the 11-year solar cycle and CO_2 doubling, *J. Clim.*, *19*(16), 3903–3931.
She, C. Y., and U. von Zahn (1998), Concept of a two-level mesopause: Support through new lidar observations, *J. Geophys. Res.*, *103*, 5855–5863.
She, C.-Y., S. Chen, Z. Hu, J. Sherman, J. D. Vance, V. Vasoli, M. A. White, J. Yu, and D. A. Krueger (2000), Eight-year climatology of nocturnal temperature and sodium density in the mesopause region (80 to 105 km) over Fort Collins, CO (41°N, 105°W), *Geophys. Res. Lett.*, *27*(20), 3289–3292.
Shepherd, M. G., Y. J. Rochon, D. Offermann, M. Donner, and P. J. Espy (2004), Longitudinal variability of mesospheric temperatures during equinox at middle and high latitudes, *J. Atmos. Sol. Terr. Phys.*, *66*, 463–479, doi:10.1016/j.jastp.2004.01.036.
Thomas, G., J. Olivero, M. DeLand, and E. Shettle (2003), Comment on "Are noctilucent clouds truly a miner's canary for global change?", *Eos Trans. AGU*, *84*(36), 352–353.
von der Gathen, P. (1991), Saturation effects in Na lidar temperature measurements, *J. Geophys. Res.*, *96*, 3679–3690.
von Zahn, U. (2003), Are noctilucent clouds truly a "miner's canary" for global change?, *Eos Trans. AGU*, *84*(28), 261–264.
von Zahn, U., and J. Höffner (1996), Mesopause temperature profiling by potassium lidar, *Geophys. Res. Lett.*, *23*, 141–144.
von Zahn, U., J. Höffner, V. Eska, and M. Alpers (1996), The mesopause altitude: Only two distinctive levels worldwide?, *Geophys. Res. Lett.*, *23*, 3231–3234.

J. Höffner and F.-J. Lübken, Leibniz-Institute of Atmospheric Physics, Schloss-Str. 6, D-18225 Kühlungsborn, Germany. (hoeffner@iap-kborn.de)